POLITECNICO DI TORINO
Repository ISTITUZIONALE

Nanocrystalline Cellulose from the Solitary Tunicate Phallusia Mammillata, a Valuable Nanocellulose Precursor

Original
Nanocrystalline Cellulose from the Solitary Tunicate Phallusia Mammillata, a Valuable Nanocellulose Precursor / Riccioni, A., Famengo, A., El Habra, N., Ballarin, L., Manni, L., Zamuner, A., Schievano, E.. - In: ADVANCED SUSTAINABLE SYSTEMS. - ISSN 2366-7486. - 9:8(2025), pp. 1-9. [10.1002/adsu.202500139]

Availability:
This version is available at: 11583/3006808 since: 2026-01-22T08:47:00Z

Publisher:
John Wiley and Sons

Published
DOI:10.1002/adsu.202500139

Terms of use:

This article is made available under terms and conditions as specified in the corresponding bibliographic description in the repository

Publisher copyright

(Article begins on next page)

26 November 2026

Check for updates

ADVANCED SUSTAINABLE SYSTEMS
www.advsustainsys.com

Nanocrystalline Cellulose from the Solitary Tunicate *Phallusia Mammillata*, a Valuable Nanocellulose Precursor

Andrea Riccioni, Alessia Famengo, Naida El Habra, Loriano Ballarin, Lucia Manni, Annj Zamuner, and Elisabetta Schievano*

Ascidians are ubiquitous filter-feeding marine invertebrates, the only animals producing cellulose in their outer tunic, in the form of a composite structure of cellulose microfibrils linked to a protein matrix. This study reports the successful processing of *Phallusia mammillata*, a species prevalent in the Northern Adriatic Sea, into high-quality nanocellulose (NC). An optimized extraction method followed by chemical modification is applied to produce suitable precursors for cellulose-based products. Structural, compositional, and thermal characterization demonstrated the high degree of crystallinity of the extracted cellulose, which is further processed into both cationic and anionic forms by direct reaction of nanofibril suspensions. High-aspect-ratio nanofibrillated cellulose (NFC) with a fibrils diameter of 10 ± 2 nm is directly obtained from purified tunics. Anionic nanocrystals and cationic nanofibrils with a mean diameter of 8 ± 2 nm are obtained from pristine nanofibrillated cellulose suspensions. To the best of the authors' knowledge, this is the first report on the extraction and processing of cellulose from *Phallusia mammillata*, opening new possibilities toward high-grade cellulose-based materials exploiting an abundant local resource.

1. Introduction

Cellulose is the most abundant biopolymer on Earth, synthesized by all plants, algae, bacteria, and a group of marine invertebrates, the tunicates. Native cellulose chains aggregate into fibrils yielding complex architectures of crystalline, paracrystalline/amorphous domains depending on the biosynthesis path.[1] Most of the native cellulose are found as two allomorphs of a crystallographic phase referred as cellulose I, I_α (triclinic, P1 space group), and I_β (monoclinic, P2 space group). Recently, Brouwer and Mikolajewskji identified a third polymorph labeled as I_β for bacterial cellulose.[2]

Tunicates contain cellulose in their external body layer, the tunic, which can be extracted and purified from proteins, lipids, and related derivatives by acidic and basic hydrolysis steps. Similar to plant cellulose, tunicate cellulose (TC or tunicin) aggregates in the form of microfibrils composed of a nearly pure cellulose I_β allomorph.[3–5] Furthermore, pristine cellulose from tunicates is not associated with lignin or hemicellulose as for plant sources, the latter less prone toward their deconstruction because of several macroscopic and microscopic factors, tissue heterogeneity, and the very strong lignin-carbohydrates interaction, requiring prior thermochemical pretreatments such as Kraft pulping.[6] In general, TC has a higher crystallinity and aspect-ratio than wood cellulose (WC) an important feature for biomedical applications, optoelectronics, sensors, and catalysis.[7–9] Ascidians, the main group of tunicates, are abundant in shallow waters and grow as sessile animals on different kinds of hard substrates, even of anthropogenic origin.[10]

Improvements have been made toward the scalable isolation of cellulose from different tunicate species, including invasive varieties. This progress presents a potential strategy to mitigate the detrimental effect of invasive tunicates on global aquaculture communities and provides a valuable sustainable resource for various industrial applications.[4, 11–14] The growing interest in cellulose isolation from non-wood and non-plants sources is prompted by the rising demand for the so-called nanocellulose (NC), a highly crystalline cellulose in the nanometric form.[15]

Although the structure and morphology of NC are determined by the synthesis process, current research highlights different

A. Riccioni, E. Schievano
Department of Chemical Sciences
University of Padova
Padova 35121, Italy

A. Famengo, N. El Habra
Institute of Condensed Matter Chemistry and Technologies for Energy
National Research Council of Italy
Padova 35127, Italy
E-mail: alessia.famengo@cnr.it

L. Ballarin, L. Manni
Department of Biology
University of Padova
Padova 35131, Italy

A. Zamuner
Department of Civil
environmental and Architectural engineering
University of Padova
Padova 35131, Italy

The ORCID identification number(s) for the author(s) of this article can be found under https://doi.org/10.1002/adsu.202500139

© 2025 The Author(s). Advanced Sustainable Systems published by Wiley-VCH GmbH. This is an open access article under the terms of the Creative Commons Attribution License, which permits use, distribution and reproduction in any medium, provided the original work is properly cited.

DOI: 10.1002/adsu.202500139

23667486, 2025, 8, Downloaded from https://advanced.onlinelibrary.wiley.com/doi/10.1002/adsu.202500139 by Politecnico Di Torino Sist. Bibl Del Polit Di Torino, Wiley Online Library on [22/01/2026]. See the Terms and Conditions (https://onlinelibrary.wiley.com/terms-and-conditions) on Wiley Online Library for rules of use; OA articles are governed by the applicable Creative Commons License

structural, compositional, and optical properties of final materials depending on the raw sources. As an example, cellulose fibers from bast are characterized by a long fiber length, if compared to other biomasses, possessing strong mechanical properties.[16] Widening NC production from conventional plant-based sources to tunicates can, in principle, broaden the material applications field.[3] In this context, the aim of this work is to set up a simple and cost-effective extraction procedure of nanofibrillated cellulose (NFC) from the solitary ascidian *Phallusia mammillata* to obtain highly pure and crystalline cellulose to be converted into valuable and nanometer-scale cationic and anionic cellulose precursors. *P. mammillata* is common in the Northern Adriatic Sea, usually 10–14 cm long, and has a whitish, very thick, smooth tunic, forming numerous rounded protuberances. This organism colonizes hard substrates, including mussel shells and, therefore, is commonly discarded as waste by mussel farmers when preparing the product for sale. It can be regarded as a local precursor of high-grade cellulose: to the best of the authors' knowledge, the exploitation of tunicin from *P. mammillata* has not been reported yet.

A detailed compositional and structural characterization is described to assess the modifications introduced upon NFC chemical processing, pivotal for its exploitation as a natural biomaterial. NFC was chemically modified by periodate oxidation, a method of polysaccharides derivatization yielding two aldehydes moieties at both C2 and C3 of the glucopyranose ring commonly referred as dialdehyde cellulose (DAC) or periodate-oxidized cellulose (POC) which can be further oxidized to give anionic dicaboxylic cellulose (Ox-DAC).[17, 18] Surface modification of NFC using positively charged derivatives was achieved via etherification with a quaternary ammonium epoxide (2,3-EpoxyPropyl Trimethyl Ammonium Chloride–EPTMAC) to obtain EPTMAC-NFC as a precursor for biomaterials with antimicrobial properties and with affinity for proteins or enzymes.[19–21] Anionic Sulphated-Cellulose NanoCrystals (S-CNC) were obtained upon NFC acidic hydrolysis.

2. Results and Discussion

2.1. Cellulose Extraction and Characterization

P. mammillata is an ascidian that can be easily found in the Northern Adriatic Sea attached to hard substrata, such as ropes, boat bottoms, and both wood and stone docks. It reproduces in spring and autumn, reaching an average length of 12.3 cm and an average weight of 65.25 g. External fertilization and larval growth ensure a constant population of animals that can be harvested for laboratory experiments without requiring ethical approval. Although cellulose from different tunicate species is generally highly pure and crystalline with the predominant I_β phase, microfibrils size and aggregation vary within the species. Several studies on cellulose from species of the genera *Halocynthia, Styela, Ciona, Ascidia*, and *Metandroxapa* are reported in the literature.[14] However, few papers describe cellulose extraction from *Phallusia*, focusing on solitary tropical *P. nigra*.[22] About 100 animals were used to obtain the tunics (Figure S1, Supporting Information), which account for slightly above half of the specimen weight (58%) containing an average water content of 93.5%. The extraction yield of NFC was ≈1% of the whole animal weight.

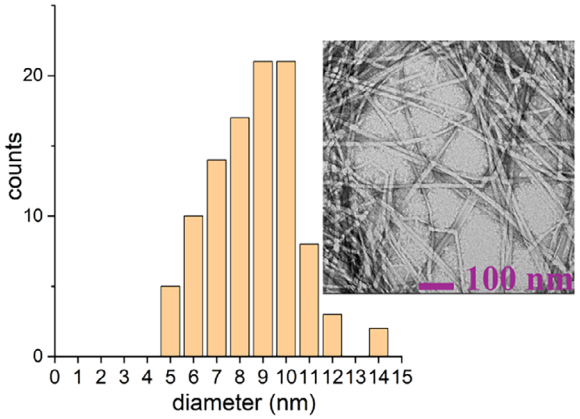

Figure 1. TEM micrographs of NFC suspension and calculated diameter distribution.

High shear stirring was found to be effective for a more homogeneous and easily processable suspension, containing 0.2 wt.% of cellulose, which can be freeze-dried to obtain fibers or directly used for chemical functionalization reactions.

NFC suspensions are constituted by interwoven fibers several micrometers long (Figure S2, Supporting Information), this microstructure being consistent with the intrinsic high crystallinity and aspect-ratio of pristine tunics, constituted by microfibrils bundles present as multilayers on the animal epidermis.[23]

The morphology of the cellulose extracted from *P. mammillata* is similar to that observed for celluloses from *Ascidia sp.* and *Ciona. intestinalis*.[14] A semi-quantitative evaluation of fiber diameters can be done by means of TEM microscopy: representative micrographs of NFC fibrils together with the calculated diameter distribution are reported in **Figures 1** and S3 (Supporting Information). A mean diameter value of 10 ± 2 nm and median of 10 nm indicates that the homogenization process was somewhat effective in reducing the aggregation of fibril bundles in NFC. Due to the absence of any visible break in the 100 and 500 nm windows of TEM images (Figure 1; Figure S3, Supporting Information), it is reasonable to estimate a fiber length greater than 500 nm, corresponding to an aspect ratio greater than 50 calculated from a mean diameter of 10 nm.

In the literature, there is no global consensus on the classification of different nanocellulose morphologies, this term covering a wide range of particle types, from well-defined and monodisperse nanometric crystals to polydisperse aggregated fibrils with diameter in the nm-scale.[15] However, here we will consider the cellulose extracted from *P. mammillata* as nanofibrillated cellulose following the definition of the Canadian Standard Association and proposed by Benselfelt and co-workers, referring to NFC as a cellulosic object composed of at least one primary fibril (dimensions typically 3–15 nm in cross-section), containing crystalline and amorphous regions, with aspect ratio usually greater than 50, which may exhibit longitudinal splits, entanglement between cellulose nanofibrils or network-like structure".[15]

All the characteristic peaks of cellulose were detected by FT-IR analysis of freeze-dried NFC (**Figure 2a**, **Table 1**).

© 2025 The Author(s). Advanced Sustainable Systems published by Wiley-VCH GmbH

23667486, 2025, 8, Downloaded from https://advanced.onlinelibrary.wiley.com/doi/10.1002/adsu.202500139 by Politecnico Di Torino Sist. Bibl Del Polit Di Torino, Wiley Online Library on [22/01/2026]. See the Terms and Conditions (https://onlinelibrary.wiley.com/terms-and-conditions) on Wiley Online Library for rules of use; OA articles are governed by the applicable Creative Commons License

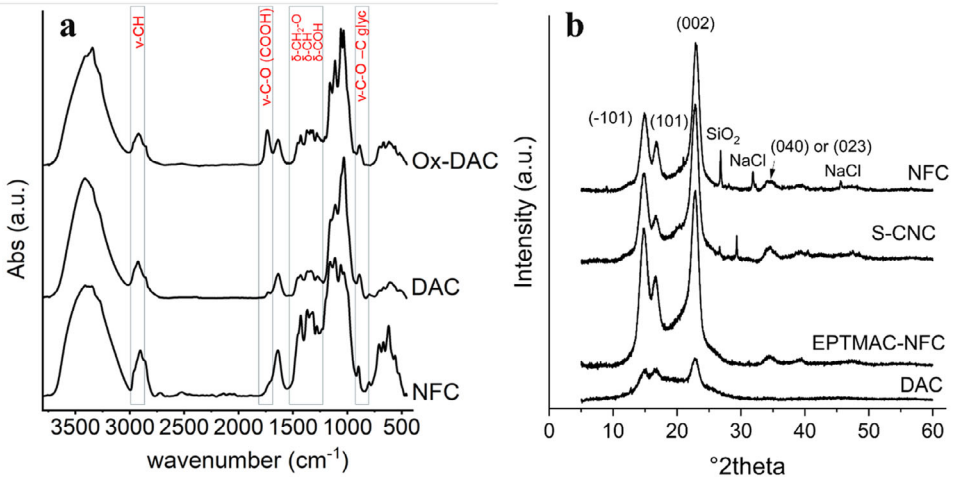

Figure 2. a) FT-IR spectra of NFC, of periodate oxidized NFC (DAC), and of periodate-chlorite oxidized cellulose Ox-DAC; b) XRD patterns of NFC, S-CNC, cationic EPTMAC-NFC, and DAC.

In particular, the region between 1450 and 1200 cm^{-1} contains various contributions related to the bending of CH_2 bonds, CH bonds, and COH bonds, the weak band at 898 cm^{-1} is the vibration of the glycosidic bond in the amorphous regions of the material and, finally the band at ca 1640 cm^{-1} is due to the presence of moisture within the sample.[24–27]

The crystal structure of freeze-dried NFC samples was studied by XRD analyses. The diffraction pattern of NFC shown in Figure 2b is composed of amorphous and crystalline regions: four main reflection characteristics of cellulose I_β are visible at 2θ values 14.2°(1–10), 16.8° (110), 22.9°(002), and the wide low-intensity reflection centered at ≈34.5°, resulting from the overlapping of several minor reflection, generally associated to crystallographic planes (004) or (023), characteristics of the crystal polymorph I_β.[28, 29] Some residual impurities are visible at 2θ = 26.7°, corresponding to the main reflection of hexagonal silicon dioxide (SiO_2) in quartz phase (ICDD: 01-074-1811) and cubic NaCl (Figure 2b).

The crystallinity index (CI) extrapolated by XRD patterns is 90.7%, revealing a high crystallinity confirmed by the sharpness of the main reflection at ≈22.9°. However, with the employed estimation method I_{am} values can be significantly underestimated, leading to an overestimation of the CI.[30] The crystallite size calculated on (002) diffraction plane is 69 Å, consistent with the value of 72.3 Å for tunicate Styela clava cellulose.[14]

Crystalline, para-crystalline and amorphous contributions are revealed by ^{13}C CP-MAS NMR, one of the main techniques for the structural characterization of cellulosic materials and quantification of crystalline ratio. The relative intensities of ^{13}C-detected resonances are quantitative, providing an adequate contact time, because of the intrinsic rigid nature of cellulose molecules, originating from the intermolecular hydrogen bonding, and for the presence of protons bonded to each C atom.[31] The CI calculated on C4 is 75%; the amount of non-crystalline cellulose calculated from the mixed Gaussian/Lorentzian peak of the C1 region at 105.38 ppm can be considered similar to the value obtained by integrating the broad C4 peak at 84.14 ppm (Table S1, Supporting Information), coherently with the fact that the two AGU units are linked through C1—C4 bonds. **Figure 3** reports ^{13}C-CP-MAS NMR spectrum and its deconvolution for NFC, showing the presence of I_β phase as the only allomorph.[32]

Crystallinity of cellulosic materials can affect their thermal degradation behavior, an important factor for their different applications. The thermal stability of cellulose nanofibrils extracted was evaluated by TGA-DTG shown in **Figure 4**.

Adsorbed H_2O is lost in the RT-150 °C range, accounting for almost a 3% loss of the initial mass for both NFC and the pristine tunic, cleared from lipids, proteins, and non-cellulosic components. As evidenced by DTG curves, the two celluloses have different patterns in the 150–550 °C interval: a sharp peak at 349.3 °C with a broad band at ≈ 270 °C observed for NFC and a single and broader peak for pristine tunics at 334 °C. Deconvolution of NFC DTG (Figure S8, Supporting Information) resulted in five different peaks for cellulose degradation: the broad peak at 287.0 °C is attributable to the fraction of cellulose particles with higher surface area and non-crystalline domains (as evidenced

Table 1. Characteristic FT-IR absorption bands for NFC, periodate oxidized DAC, and periodate-chlorite oxidized Ox DAC samples.[20, 28–30]

	NFC	DAC[c]	Ox-DAC [d]
ν-OH	3300 cm^{-1} (vs)	3415 cm^{-1} (vs)	3415 cm^{-1} (vs)
ν-CH	2900 cm^{-1} (ms)	2925 cm^{-1} (ms)	2925 cm^{-1} (ms)
ν-C-O (COOH)	–	–	1736 cm^{-1} (ms)
δ-CH_2 δ-CH δ-COH	1450 to 1200 cm^{-1}	1450 to 1200 cm^{-1}	1450 to 1200 cm^{-1}
glycosidic bond	1150 cm^{-1} (s)	1152 cm^{-1} (s)	1159 cm^{-1} (s)
ν- CO	1100 cm^{-1} (s)	1112 cm^{-1} (s)	1115 cm^{-1} (s)
ν- COC	1030 cm^{-1} (s)	1030 cm^{-1} (s)	1035 cm^{-1} (s)
ν-COC glyc	898 cm^{-1} (w)	892 cm^{-1} (w)	892 cm^{-1} (w)

© 2025 The Author(s). Advanced Sustainable Systems published by Wiley-VCH GmbH

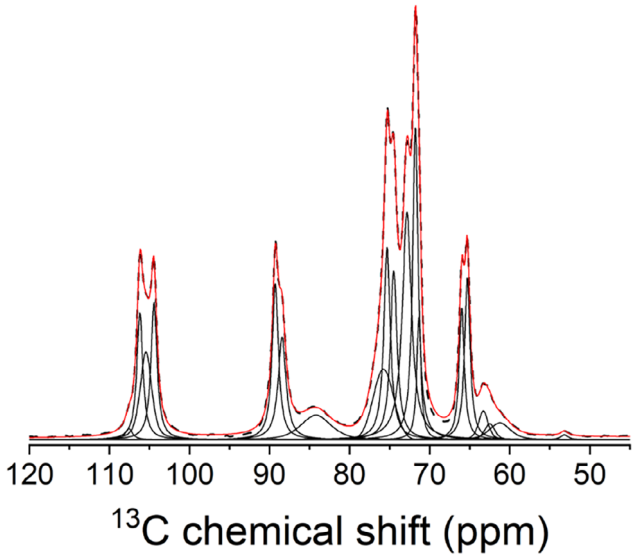

Figure 3. Experimental (black dashed) and model spectra (red) resulting from the different contributions obtained by deconvolution into Lorentzian/Gaussian line shapes for NFC. Fitting details in Table S1 (Supporting Information).

by ^{13}C CP-MAS NMR), whose thermal stability is lower than for crystalline cellulose.[33]

The presence of nanofibrils is also evidenced by the lower temperature at 10% sample degradation observed for NFC (T = 284.3 °C), compared to the one for pristine tunics (T = 301.7 °C). The cellulose decomposition mechanisms in N_2 are reflected by four peaks in the 320–450 °C temperature range of the deconvoluted DTG curve (Figure S8, Table S4, Supporting Information), involving cellulose dehydration, dehydrocellulose decomposition into volatiles and char, cellulose depolymerization, and thermal auto-oxidation at temperatures exceeding 400 °C. Char content at 800 °C is similar for both samples, 19.07% for tunics and 18.69%

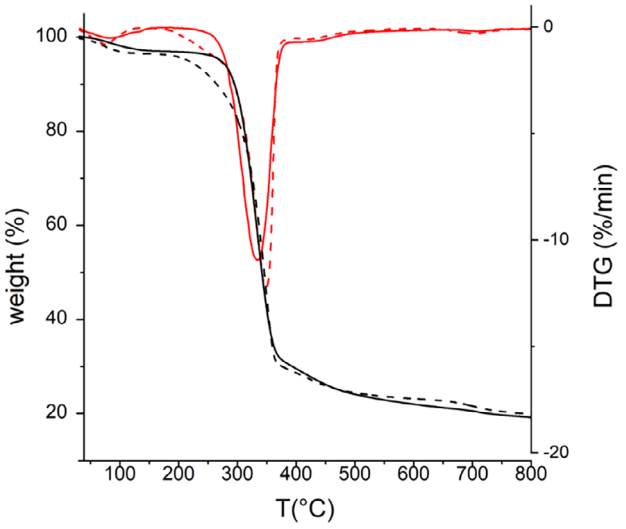

Figure 4. TGA (black) and DTG (red) curves for pristine tunic precursor (solid) and NFC (dashed).

for NFC. As evidenced by XRD analysis, the presence of inorganic contaminants such as NaCl and SiO_2 contributed to the residual mass at 800 °C. Furthermore, as reported in literature, tunicates are filter-feeding animals and they usually embed inorganic salts and heavy metals from the environment.[4, 7]

2.2. Chemical Modification of NFC Obtained from *P. mammillata*

The reactivity of NFC extracted from *P. mammillata* is assessed for the first time by typical chemical modification methods of polysaccharides: oxidation to aldehydes with $NaIO_4$ and $NaIO_4/NaClO_2$, and cationization with 2,3-epoxypropyltrimethylammonium chloride (EPTMAC) to introduce functional groups along the glycosidic chain that could be used as grafting point for other functionalization strategies. Few papers report on the cationic functionalization of tunicate cellulose.[34, 35] A hydrolysis test of the NFC suspension was also performed, with the aim of producing tunicate nano-cellulose characterized by lower longitudinal dimensions.

Hydrolysis of NFC extracted from *P. mammillata* with 62 wt.% H_2SO_4 yields cellulose with a morphology distinct from the extracted pristine material, as revealed by TEM micrographs of **Figures 5** and S4 (Supporting Information). The resulting material exhibits a more heterogeneous distribution of fibril lengths and a reduced tendency to aggregate, supporting its easy suspension in water to form stable colloids, due to the presence of charged SO_4^- groups on the surface. In contrast, the precursor NFC fibers showed a greater propensity for aggregation and precipitation. Cellulose fibrils exhibit a mean diameter of 8 ± 2 nm, with ≈65% of the analyzed fibers having an aspect ratio <50. Note that the aspect ratio distribution is broad due to the coexistence of both "short" (<500 nm) and long (>500 nm) fibrils. However, to highlight the difference with pristine NFC, here we refer to sulfated celluloses as S-CNC (sulfated-cellulose nanocrystals), despite the presence of a non-negligible fraction of fibers with a high aspect ratio.

The fibers high aspect ratio was maintained after the reaction of pristine NFC with EPTMAC (**Figure 6**), but the fibrils were less aggregated, as expected when a charged group is introduced: as for S-CNC, EPTMAC-NFC formed stable colloidal suspensions. Like pristine NFC, it was not possible to measure fiber length by TEM (Figure 6, Figure S5, Supporting Information) because no breaks were observed, suggesting a fibril size of several micrometers. A mean diameter of 8 ± 2 nm was calculated.

It is important to note that, in this case, the reaction was effective directly on NFC dispersions, avoiding the hydrolysis step.[33, 34] In fact, chemical functionalization in dispersion is more difficult for NFC than for CNC due to the NFC tendency to entangle and aggregate.[15] Furthermore, to date, tunicin cationization was usually carried out on nanocrystals colloids.[34, 35]

The ^{13}C CP-MAS NMR spectra shows that the sulfuric acid hydrolyzed cellulose nanocrystals (S-CNC) (Figure S6, Table S2, Supporting Information) have both crystalline and non-crystalline/paracrystalline contributions, similar to the pristine nanofibrillated cellulose (NFC) precursor.

The normalized ^{13}C-CP-MAS spectra of S-CNC and NFC are almost overlapping (Figure 7), indicating the acid hydrolysis preserves the crystallinity of the original NFC. The crystallinity index

© 2025 The Author(s). Advanced Sustainable Systems published by Wiley-VCH GmbH

23667486, 2025, 8, Downloaded from https://advanced.onlinelibrary.wiley.com/doi/10.1002/adsu.202500139 by Politecnico Di Torino Sist. Bibl Del Polit Di Torino, Wiley Online Library on [22/01/2026]. See the Terms and Conditions (https://onlinelibrary.wiley.com/terms-and-conditions) on Wiley Online Library for rules of use; OA articles are governed by the applicable Creative Commons License

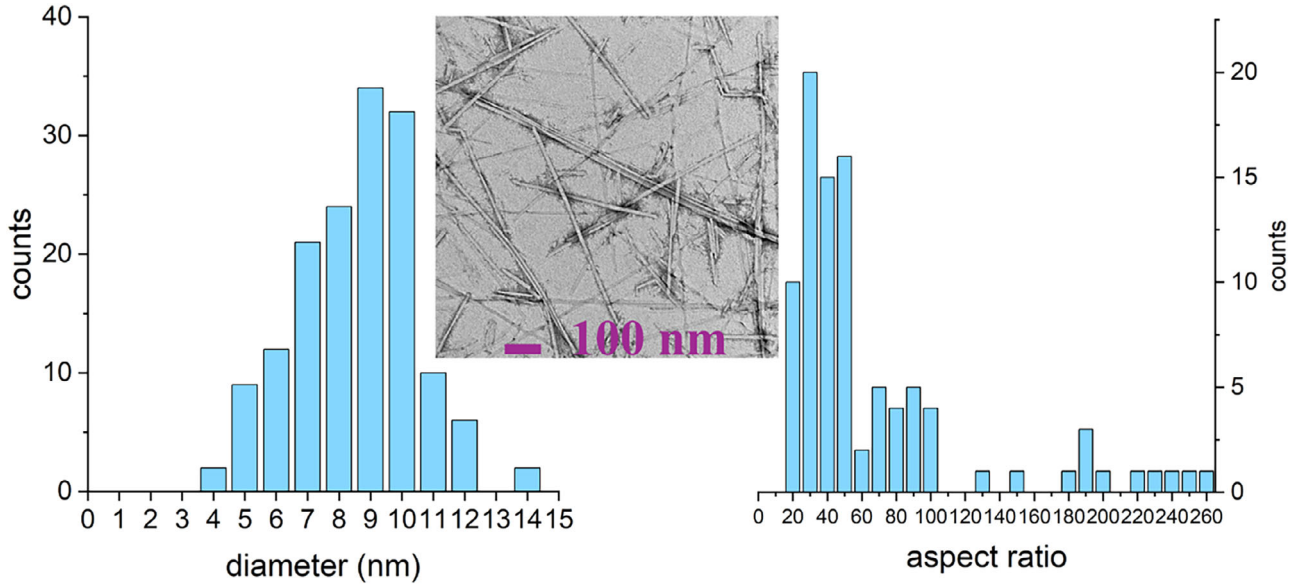

Figure 5. TEM micrograph of S-CNC obtained from NFC hydrolysis with diameter and aspect ratio distributions.

calculated from the C4 peak is ≈72% for S-CNC, slightly lower than 75% for NFC.

The acid treatment helps removing residual protein/lipid impurities, as seen by the lower intensity signals in the 0–40 ppm range for S-CNC compared to NFC.

XRD data further confirms that H_2SO_4 hydrolysis does not significantly alter the original crystal structure of NFC cellulose. The high crystallinity (CI of 85%) is confirmed by the sharpness of the main reflection at ≈22.9°.

However, at high H_2SO_4 concentrations, a small fraction of crystalline cellulose is expected to undergo hydrolysis, leading to partial damage of the crystalline structure and a lower crystalline index.[28, 36]

The crystallite size calculated on (002) is 71 Å, a value comparable to that of the parent NFC. High crystallinity was preserved even after quaternization of NFC cellulose with EPTMAC, as evidenced by both CP-MAS NMR (**Figure** 7; Figure S7, Table S3, Supporting Information) and XRD (Figure 2b) analysis. The CI was found to be 81% and 80%, respectively, with an estimated crystallite dimension of 71 Å (from XRD). The presence of $[N(CH3)_3]^+$ moiety is confirmed by the peak at 55.73 ppm in the ^{13}C CP-MAS spectrum, assigned to the methyl carbons of the quaternary ammonium.[37] A degree of substitution (DS) of 0.02 was calculated from the peak area ratio ($N(CH3)_3$ /3)/(C1).

NFC was successfully oxidized to dialdehydic cellulose (DAC) by $NaIO_4$, followed by $NaClO_2$ oxidation of the aldehydic groups into carboxylates (Ox-DAC): as widely reported in literature aldehydes signals are not detected neither by ^{13}C CP-MAS NMR in the 160–200 ppm range as usually expected, neither via FT-IR

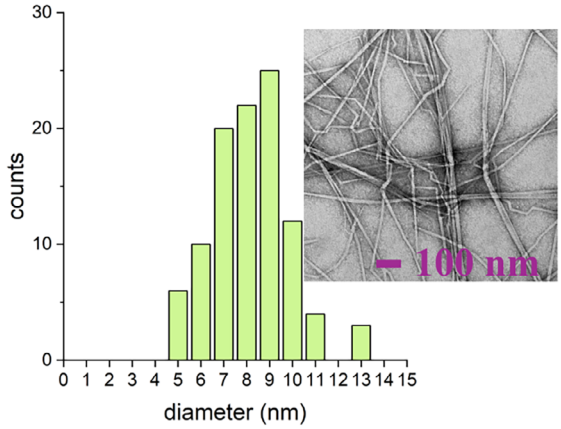

Figure 6. TEM micrograph of TEM micrograph of EPTMAC-NFC with related diameter distribution.

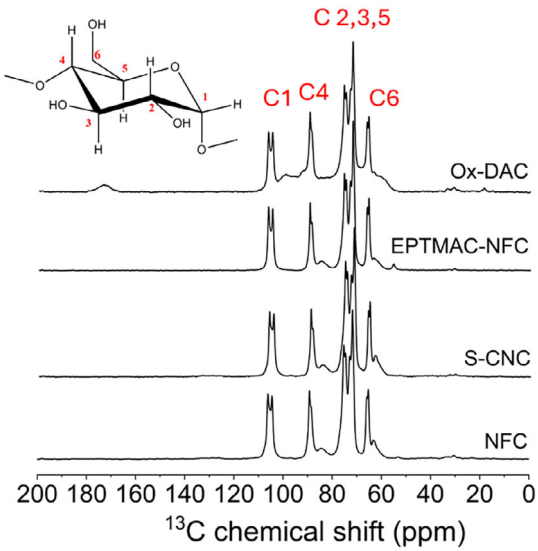

Figure 7. Comparison of normalized ^{13}C CP-MAS spectra in the 0–200 ppm range of NFC, S- CNC, cationic EPTMAC-NFC, and NaClO2 oxidized DAC (Ox-DAC).

© 2025 The Author(s). Advanced Sustainable Systems published by Wiley-VCH GmbH

23667486, 2025, 8, Downloaded from https://advanced.onlinelibrary.wiley.com/doi/10.1002/adsu.202500139 by Politecnico Di Torino Sist. Bibl Del Polit Di Torino, Wiley Online Library on [22/01/2026]. See the Terms and Conditions (https://onlinelibrary.wiley.com/terms-and-conditions) on Wiley Online Library for rules of use; OA articles are governed by the applicable Creative Commons License

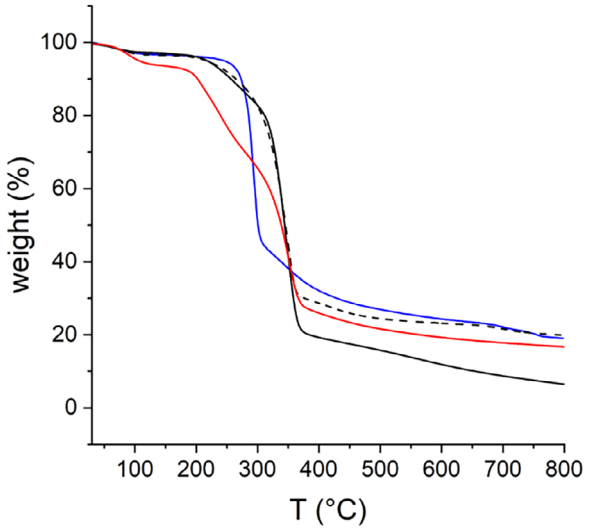

Figure 8. TGA curves of: S-CNC (blue); EPTMAC-NFC (black, solid), Ox-DAC (red), and NFC (black, dashed).

(Figure 2a, Table 1), with the absence of the characteristic strong carbonyl absorption band ≈1730 cm^{-1}.[17] This is likely due to the conversion of aldehydes into hydrated aldehydes, intra- and inter-molecular hemiacetals, and aldals.[38–40] However, $NaClO_2$ converts "masked" aldehydes functionalities into carboxylic acid groups,[38] detectable by both FT-IR and ^{13}C CP-MAS NMR. FT-IR spectrum of Ox-DAC (Figure 2a, Table 1) shows a well-distinct peak at 1736 cm^{-1} which is the protonated form of carboxyl groups, detected as a new signal at 175 ppm by ^{13}C CP-MAS NMR spectrum (Figure 7).[41] In addition, the effect of $NaClO_2$ oxidation was to broaden the ^{13}C NMR of Ox-DAC in the 80–100 ppm region: this can be due to an increase of the amorphous content but also to the presence of residual masked aldehydes, partially overlapping to cellulose C4 and C1 signals and to some extent, to C6 signals. The complexity of the ^{13}C CP-MAS NMR spectrum of dialdehyde cellulose (DAC) made crystallinity determination inaccurate. Therefore, it was calculated from XRD, showing a reduced CI of 50% and crystallite size of 3.9 nm for DAC, consistent with the expected decrease in crystallinity upon oxidation reported in literature.[39]

Analysis of the TGA-DTG curves (**Figure 8**; Figure S8, Supporting Information) allows a direct comparison between the samples carrying different functional groups. In the RT-150 °C region, adsorbed water is observed for all the samples, as indicated by the broad DTG peak ≈100 °C. The effect of chemical composition (i.e., the presence of functional groups) and micro/nanostructural features of cellulose on its thermal behavior can be observed in the 150–500 °C region.

The thermal decomposition pattern of parent NFC was modeled by DTG deconvolution (Figure S8, Table S4, Supporting Information) into multiple peaks: the wide Gaussian at 287.03 °C corresponds to the degradation of the amorphous-semicrystalline fraction of cellulose, while peaks at 326.63, 344.08, and 355.28 °C are attributable to the to the different chemical processes involved in cellulose chemical composition, such as depolymerization and dehydration, decomposition of glycosyl units and the formation of a charred residue. A further broad peak at 424.17 °C is an indication of the pyrolysis of charred residue into lighter compounds.

The DTG profile of EPTMAC-NFC showed a first peak at 258.40 °C, the decomposition of the cationic groups. After this temperature, the DTG pattern is similar to the one for pristine NFC, with the presence of 4 peaks (339.20, 350.0, 363.30, and 372,1 °C) indicating the degradation of amorphous-semicrystalline domains at 339.20 °C, followed by the 3 peaks decomposition profile of crystalline cellulose, as for NFC.

S-CNC decomposition pattern shows a sharp DTG peak at 294.3 °C and a very broad and weak band at ≈350 °C.

DTG curve deconvolution of S-CNC into three main components (Figure S8 and Table S4, Supporting Information) yielded three different degradation processes at 285.5, 294.61, and 336.9 °C. The first peak is attributable to the amorphous fraction of sulfated cellulose nanocrystals while the second peak is the degradation of the crystalline domains. The first peak temperature is higher than the degradation temperature of 200 °C reported for the cellulose desulfation process, leading to H2SO4 elimination, which in turn can catalyze cellulose dehydration, as observed for sulfated bacterial nanocellulose.[42] The higher stability of S-CNC can be explained by H+ counterions exchange with Na+ in the SO3- moiety, preventing the acid-catalyzed cellulose dehydration and shifting the degradation temperature of Na-CNC at ≈100 °C higher than the H+-CNC, similar to what observed by D'Acierno et al., for sulfated cellulose nanocrystals.[43]

In Ox-DAC the stability onset is at T = 192 °C and the DTG deconvolution revealed two peaks at 205.9 and 239.1 °C (Figure S8, Table S4, Supporting Information), accounting for a mass loss of 30% of the initial weight. The TGA and DTG patterns observed in this study are similar to those reported in literature for fully dicarboxylic cellulose from DAC oxidation, where more than 50% of weight loss occurs in the RT-250 °C range.[44] The lower mass loss is due to the fact that not all the AGU units are oxidized in Ox-DAC. The decomposition pattern from 300 to 500 °C resembles that of pristine NFC, with cellulose degradation occurring via different mechanisms, with the peak at 316.04 °C corresponding to the amorphous-paracrystalline cellulose fraction.

Analysis of the DTG peaks area of NFC, S-CNC, and EPTMAC-NFC (Figure S8, Table S4, Supporting Information) provides a semiquantitative estimation of cellulose crystallinity, as its thermal stability depends also on the presence of amorphous and/or paracrystalline fractions which can be deconvoluted into one or more peaks.[45]

The area of lower temperature peaks corresponds to amorphous/paracrystalline cellulose domains in the absence of other plant components (hemicelluloses, lignin, and extractives).

The DTG crystallinity values, reported in **Table 2**, are consistent with those obtained from NMR, with differences arising from the presence of minor impurities and the earlier degradation of part of the cellulose backbone involved in the cationic functional group degradation.

3. Conclusion

This work reported, for the first time, the extraction and functionalization of highly pure and crystalline nanocellulose from *P. mammillata*, a solitary ascidian common in the Northern

© 2025 The Author(s). Advanced Sustainable Systems published by Wiley-VCH GmbH

23667486, 2025, 8, Downloaded from https://advanced.onlinelibrary.wiley.com/doi/10.1002/adsu.202500139 by Politecnico Di Torino Sist. Bibl Del Polit Di Torino, Wiley Online Library on [22/01/2026]. See the Terms and Conditions (https://onlinelibrary.wiley.com/terms-and-conditions) on Wiley Online Library for rules of use; OA articles are governed by the applicable Creative Commons License

Table 2. Comparison of cellulose crystalline fraction evaluated by three different analytical techniques: first derivative of the thermogravimetric curves (DTG), NMR, and XRD.

Crystallinity	%DTG	%NMR	%XRD
NFC	74	75	91
S-CNC	67	72	80
EPTMAC-NFC	70	81	80

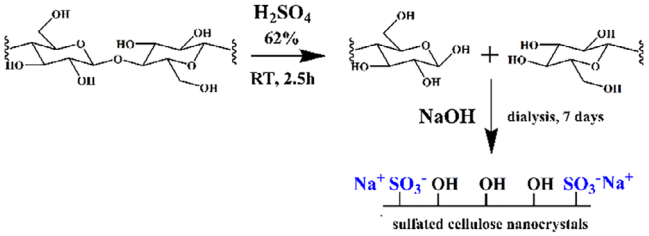

Scheme 1. NFC hydrolysis with H_2SO_4.

Adriatic Sea. This tunicate reproduces twice a year (in spring and autumn, depending on seawater temperature) and can be commonly found attached to hard substrates, such as mussel nets usually considered as waste in mussel farming operations.

NFC from *P. mammillata* was successfully obtained through a chlorinated-free extraction procedure. The chemical nature of the extracted material, characterized by high crystallinity, was confirmed using FT-IR, SS-NMR, and XRD techniques. Acid hydrolysis of the obtained NFC modified the morphology of the material and its thermal proprieties due to the introduction of sulfate half-ester groups along the glycosidic chains. *Phallusia*-derived NFC was successfully subjected to $NaIO_4$ oxidation and EPTMAC grafting to obtain cationic cellulose. Dialdehydic cellulose formation was confirmed through a second oxidation step using sodium chlorite. The aldehydic groups were effectively oxidized to carboxylic acids, as detected by both SS-NMR and FT-IR and DTG. The oxidation was further confirmed by a decrease in the CI of DAC compared to the parent NFC.

In conclusion, we demonstrated that *P. mammillata* can be used as a valuable source of high-grade cellulose, which is easily extracted, processed, and functionalized.

4. Experimental Section

Materials: All commercially available reagents and solvents (H_2SO_4, NaOH, $NaClO_2$, CH_3COOH, THF, EPTMAC (90%), $NaIO_4$) were purchased from Sigma–Aldrich and were used without further purification.

Collection of the Raw Material and Extraction of NFC: Cellulose was extracted from the outer tissues of ≈100 specimens of *P. mammillata*. The animals were harvested in the Northern Adriatic Sea. After mechanical separation from the internal organ, tunics were thoroughly washed and soaked for one week, with daily water changes. The extraction process, designed to isolate cellulose from residual lipids and proteins, follows a modified version of the protocol proposed by He et al. (2021).[46] The tunics were cut into pieces of ≈1 × 1 × 0.2 cm^3 and immersed in a H_2SO_4 11wt.% aqueous solution. After 72 h, samples were washed several times with deionized water and then put in a 9 wt.% NaOH aqueous solution for 6 h, changing the solution after 3 h. The pieces were then rinsed several times with deionized water until neutral pH, then with milliQ water. They were shredded with a blender and then homogenized through an IKA T 25 digital ULTRA-TURRAX high shear mixer at 16.000 rpm for 10 min obtaining the final NFC suspension.

NFC hydrolysis to S-CNC: Sulfated-cellulose nanocrystals S-CNC were synthesized by slowly adding concentrated H_2SO_4 to a 0.5 wt.% NFC suspension dropwise, up to a final H_2SO_4 concentration of 62 wt.%. Hydrolysis was carried out for 2.5 h, then the solution was carefully and slowly neutralized with solid NaOH. The resulting mixture was dialyzed against deionized water for 7 days. **Scheme 1**

Cationization of NFC to EPTMAC-NFC: 35 mL of suspension containing 1 g of NFC were mixed with 65 mL of THF. After 1 h of stirring, 1.4 g of NaOH was added and the mixture was maintained at 40 °C for 30 min, then 5.5 mL of EPTMAC was added dropwise and the reaction (**Scheme 2**) was carried out for 24 h under vigorous stirring.[47] The suspension free from the organic phase was dialyzed against deionized water for 7 days.

Periodate oxidation to DAC (di-aldehydic cellulose): Sodium periodate (NaIO4) (3.96 g) was added to 150 mL of a water suspension containing 1 g of NFC. After 56 h the reaction was quenched by adding 2 mL of diethylene glycol. The suspension was then washed several times with deionized water in an ultrafiltration cell (cut-off 16 kDa).

Oxidation of Aldehyde-Functionalized NFC (DAC) with $NaClO_2$ (Ox-DAC): Aldehydic groups on periodate-oxidized cellulose were further oxidized to carboxylic moieties (**Scheme 3**). In this process, 3 mL of glacial acetic acid was added to 100 mL of water suspension containing 0.25 g of DAC. Then 0.14 g of NaClO2 was added and the reaction was carried out for 48 h under stirring. The suspension was then dialyzed against deionized water for 7 days.

Material Characterization: Transmission electron micrographs (TEM) on samples were acquired using a Tecnai G2 (FEI) transmission electron microscope at 100 kV. The images were collected by a Veleta (Olympus Soft Imaging System) digital camera. One drop of cellulose dispersion (≈25 µL) was placed on 400 mesh holey film grid; after staining with 2% uranyl acetate (for 2 min), the sample was observed operating at 120 kV. Fiber diameters and lengths were evaluated by Image J software, considering at least 100 fibers for the statistical analysis. Fourier Transformed Infrared Spectra (FT-IR) were collected on freeze-dried samples finely chopped and incorporated into KBr pellets, analyzed using a Nicolet 670 FT-IR spectrometer with a 2 cm^{-1} resolution, spectral range of 4000–400 cm^{-1}, with a total of 25 scans per sample.

The thermal stability was evaluated on freeze-dried samples by means of thermogravimetric analysis (TGA). Samples were subjected to a heating scan between 25 and 800 °C at a heating rate of 10 °C min^{-1} under N_2, with a Netzsch STA 449 F1 Jupiter Thermal Analyzer on Al_2O_3 crucibles. The inorganic residue was determined by heating under N2 (60mL min^{-1}) up to 800 °C at 10 °C min^{-1}, then cooling to 500 °C and heating to 1000 °C under air (60 mL min^{-1}). Data were processed via Netzsch Proteus Thermal Analysis software. Deconvolution of DTG curves was performed via Microcal Origin.

1D-$^{13}C\{1H\}$ MAS-NMR experiments were acquired on a Bruker Avance III spectrometer at a magnetic field strength of 7.0 T using a standard-bore probe at 23 °C. The ^1H and ^{13}C Larmor frequencies were 300 and 75.6 MHz, respectively. Freeze-dried cellulose samples were placed into a 4.0 mm ZrO_2 rotor equipped with Kel-F cap and spun at a magic-angle spinning frequency of 10 kHz. ^{13}C signals were enhanced by cross-polarization CP-MAS with 2 ms of contact time and 2.4 µs of ^1H 90° pulse,

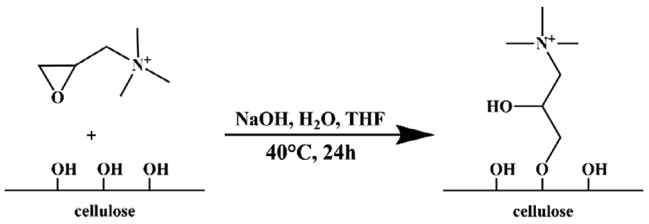

Scheme 2. NFC cationization with EPTMAC.

© 2025 The Author(s). Advanced Sustainable Systems published by Wiley-VCH GmbH

23667486, 2025, 8, Downloaded from https://advanced.onlinelibrary.wiley.com/doi/10.1002/adsu.202500139 by Politecnico Di Torino Sist. Bibl Del Polit Di Torino, Wiley Online Library on [22/01/2026]. See the Terms and Conditions (https://onlinelibrary.wiley.com/terms-and-conditions) on Wiley Online Library for rules of use; OA articles are governed by the applicable Creative Commons License

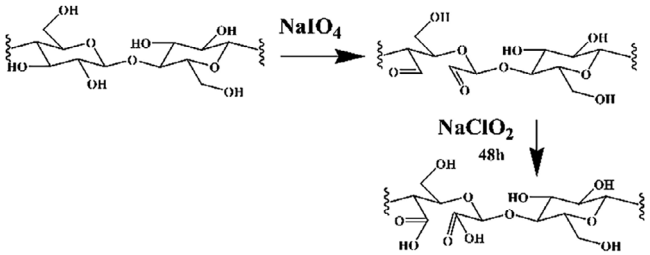

Scheme 3. Periodate-chlorite oxidation of NFC.

with SPINAL-64 proton decoupling, A 4 s recycle delay between transients was set for a number of 2000 to 4000 transients. All spectra were referenced to Adamantane at 38.48 ppm with respect to TMS. Samples were collected in dry state: even if moistening was commonly used to enhance the resolution by increasing the mobility of the system, water loss during the acquisition could not be excluded.[48] NMR data analysis, deconvolution, and fitting were carried out using Bruker TopSpin and DMfit vs64.[49]

The crystalline structure of cellulose samples was analyzed by X-ray diffraction (XRD) acquiring the patterns with a Panalytical Empyrean diffractometer in Bragg Brentano mode, equipped with a PIXcel 2D detector with a 255 × 255 array sensor, covering a solid angle 3°× 3°. The radiation was the Cu Kα (λ = 1.54056 Å) operating at 40 kV and 40 mA. All patterns were collected in the 5°÷ 60° 2θ range and the phase identification was performed with the support of the standard patterns reported in the 2002 ICDD database files. The crystallinity index (CI) for all samples was determined according to Segal's empirical method by using the following equation:

$$CI\ (\%) = \frac{(I_{002} - I_{am})}{I_{002}} x100 \quad (1)$$

where I_{200} is the intensity of the peak at ≈2ϑ = 22° corresponding to the plane (200) and representing the crystalline portion of the cellulose, while Iam is the minimum intensity value between peak (200) and peak (110) corresponding approximately to 2ϑ = 18.3° and representing the amorphous region (the intensities were calculated after subtraction of the background signal measured without cellulose).[50]

Crystallite sizes were estimated according to the Scherrer's equation calculated with respect to the main reflection (002) of I_β cellulose.

Supporting Information

Supporting Information is available from the Wiley Online Library or from the author.

Acknowledgements

This research was funded by Veneto Region, FSE project "I tunicati: da scarto nella mitilicoltura a risorsa per la Laguna di Venezia", grant number 2105-0032-553-2023 by LB, LM, ES. The authors thank Dr. F. Caicci, Manager of the Imaging Facility at the Dept. Biology, University of Padova, for TEM analysis.

Open access publishing facilitated by Consiglio Nazionale delle Ricerche, as part of the Wiley - CRUI-CARE agreement.

Conflict of Interest

The authors declare no conflict of interest.

Data Availability Statement

The data that support the findings of this study are available from the corresponding author upon reasonable request.

Keywords

ascidian, cellulose functionalization, nanocellulose, phallusia mammillata

Received: February 7, 2025
Revised: April 20, 2025
Published online: May 2, 2025

[1] P. T. Larsson, K. Wickholm, T. Iversen, *Carbohydr. Res.* **1997**, *302*, 19.
[2] D. H. Brouwer, J. G. Mikolajewski, *Cellulose* **2023**, *30*, 11341.
[3] I. A. Sacui, R. C. Nieuwendaal, D. J. Burnett, S. J. Stranick, M. Jorfi, C. Weder, E. J. Foster, R. T. Olsson, J. W. Gilman, *ACS Appl. Mater. Interfaces* **2014**, *6*, 6127.
[4] M. J. Dunlop, C. Clemons, R. Reiner, R. Sabo, U. P. Agarwal, R. Bissessur, H. Sojoudiasli, P. J. Carreau, B. Acharya, *Sci. Rep.* **2020**, *10*, 1.
[5] Y. Zhao, C. Moser, M. E. Lindström, G. Henriksson, J. Li, *ACS Appl. Mater. Interfaces* **2017**, *9*, 13508.
[6] S. P. S. Chundawat, B. S. Donohoe, L. Da Costa Sousa, T. Elder, U. P. Agarwal, F. Lu, J. Ralph, M. E. Himmel, V. Balan, B. E. Dale, *Energy Environ. Sci.* **2011**, *4*, 973.
[7] M. J. Dunlop, B. Acharya, R. Bissessur, *J. Environ. Chem. Eng.* **2018**, *6*, 4408.
[8] S. Y. Cho, H. Yu, J. Choi, H. Kang, S. Park, J. S. Jang, H. J. Hong, I. D. Kim, S. K. Lee, H. S. Jeong, H. T. Jung, *ACS Nano* **2019**, *13*, 9332.
[9] H. J. Hong, H. Yu, M. Park, H. S. Jeong, *Carbohydr. Polym.* **2019**, *210*, 167.
[10] G. Lambert, *J Exp Mar Biol Ecol* **2007**, *342*, 3.
[11] L. Marques, R. Calado, A. I. Lillebø, *Front Mar Sci* **2022**, *9*, 849870.
[12] R. J. Hickey, A. E. Pelling, *Front Bioeng Biotechnol* **2019**, *7*, 428253.
[13] R. M. A. Domingues, M. E. Gomes, R. L. Reis, *Biomacromolecules* **2014**, *15*, 2327.
[14] Y. Zhao, J. Li, *Cellulose* **2014**, *21*, 3427.
[15] T. Benselfelt, N. Kummer, M. Nordenström, A. B. Fall, G. Nyström, L. Wågberg, *ChemSusChem* **2023**, *16*, 202201955.
[16] P. Shen, Q. T., X. Chen, Z. Li, *Carbohydr. Polym.* **2022**, *290*, 119462.
[17] J. Leguy, Y. Nishiyama, B. Jean, L. Heux, *ACS Sustain Chem Eng* **2019**, *7*, 412.
[18] U. J. Kim, S. Kuga, M. Wada, T. Okano, T. Kondo, *Biomacromolecules* **2000**, *1*, 488.
[19] Y. Yang, Y. T. Lu, K. Zeng, T. Heinze, T. Groth, K. Zhang, *Adv. Mater.* **2021**, *33*, 2000717.
[20] R. J. Aguado, A. Mazega, Q. Tarrés, M. Delgado-Aguilar, *Ind. Crops Prod.* **2023**, *201*, 116898.
[21] M. Hasani, E. D. Cranston, G. Westman, D. G. Gray, *Soft Matter* **2008**, *4*, 2238.
[22] N. Chanthathamrongsiri, A. Petchsomrit, N. Leelakanok, N. Siranonthana, T. Sirirak, *Heliyon* **2021**, *7*, 07819.
[23] A. Dufresne, *Monomers, Polymers and Composites from Renewable Resources*, Elsevier, Oxford **2008**, pp. 401–418.
[24] G. Velazquez, A. Herrera-Gómez, M. O. Martín-Polo, *J. Food Eng.* **2003**, *59*, 79.
[25] S. Cichosz, A. Masek, *Materials* **2020**, *13*, 4573.
[26] A. M. Olsson, L. Salmén, *Carbohydr. Res.* **2004**, *339*, 813.
[27] E. S. Madivoli, P. G. Kareru, A. N. Gachanja, S. M. Mugo, D. S. Makhanu, *SN Appl Sci* **2019**, *1*, 723.
[28] J. Gong, J. Li, J. Xu, Z. Xiang, L. Mo, *RSC Adv.* **2017**, *7*, 33486.
[29] N. Kasyapi, V. Chaudhary, A. K. Bhowmick, *Carbohydr. Polym.* **2013**, *92*, 1116.
[30] S. Park, J. O. Baker, M. E. Himmel, P. A. Parilla, D. K. Johnson, *Biotechnol. Biofuels* **2010**, *3*, 10.

 © 2025 The Author(s). Advanced Sustainable Systems published by Wiley-VCH GmbH

23667486, 2025, 8, Downloaded from https://advanced.onlinelibrary.wiley.com/doi/10.1002/adsu.202500139 by Politecnico Di Torino Sist. Bibl Del Polit Di Torino, Wiley Online Library on [22/01/2026]. See the Terms and Conditions (https://onlinelibrary.wiley.com/terms-and-conditions) on Wiley Online Library for rules of use; OA articles are governed by the applicable Creative Commons License

[31] R. H. Atalla, D. L. Vanderhart, *The Role of Solid State 13 C NMR Spectroscopy in Studies of the Nature of Native Celluloses* **1999**.
[32] E. Malm, V. Bulone, K. Wickholm, P. T. Larsson, T. Iversen, *Carbohydr. Res.* **2010**, *345*, 97.
[33] D. Trache, A. F. Tarchoun, M. Derradji, T. S. Hamidon, N. Masruchin, N. Brosse, M. H. Hussin, *Front Chem.* **2020**, *8*, 392.
[34] P. Wei, W. Chen, Q. Song, Y. Wu, Y. Xu, *Cellulose* **2021**, *28*, 3723.
[35] T. Zhang, Q. Cheng, D. Ye, C. Chang, *Carbohydr. Polym.* **2017**, *169*, 139.
[36] W. T. Wulandari, A. Rochliadi, I. M. Arcana, *IOP Conf. Ser Mater Sci. Eng.*, Institute Of Physics Publishing, Bristol **2016**.
[37] I. A. Udoetok, L. D. Wilson, J. V. Headley, *Materials* **2016**, *9*, 645.
[38] H. Spedding, *J Chem. Soc.* **1960**, 3147.
[39] M. Siller, H. Amer, M. Bacher, W. Roggenstein, T. Rosenau, A. Potthast, *Cellulose* **2015**, *22*, 2245.
[40] I. Sulaeva, K. M. Klinger, H. Amer, U. Henniges, T. Rosenau, A. Potthast, *Cellulose* **2015**, *22*, 3569.
[41] H. Liimatainen, M. Visanko, J. A. Sirviö, O. E. O. Hormi, J. Niinimaki, *Biomacromolecules* **2012**, *13*, 1592.
[42] M. Roman, W. T. Winter, *Biomacromolecules* **2004**, *5*, 1671.
[43] F. D'Acierno, W. Y. Hamad, C. A. Michal, M. J. Maclachlan, *Biomacromolecules* **2020**, *21*, 3374.
[44] B. Pataky, S. Perczel, J.-P. Sachetto, B. A. Ttelle, *The Structural Characterization of Oxidized Celluloses by Gravimetric Analysis* **1973**.
[45] H. O. M. A. Moura, A. B. F. Câmara, L. M. A. Campos, L. S. de Carvalho, *J. Polym. Environ.* **2023**, *31*, 1915.
[46] Y. He, H. Hou, S. Wang, R. Lin, L. Wang, L. Yu, X. Qiu, *Bioact Mater* **2021**, *6*, 2000.
[47] N. Odabas, H. Amer, M. Bacher, U. Henniges, A. Potthast, T. Rosenau, *ACS Sustain Chem Eng* **2016**, *4*, 2295.
[48] L. Heux, E. Dinand, M. R. Vignon, *Carbohydr. Polym.* **1999**, *40*, 115.
[49] D. Massiot, F. Fayon, M. Capron, I. King, S. Le Calvé, B. Alonso, J. O. Durand, B. Bujoli, Z. Gan, G. Hoatson, *Magn. Reson. Chem.* **2002**, *40*, 70.
[50] L. Segal, J. J. Creely, A. E. Martin, C. M. Conrad, *Text. Res. J.* **1959**, *43*, 786.

© 2025 The Author(s). Advanced Sustainable Systems published by Wiley-VCH GmbH

23667486, 2025, 8, Downloaded from https://advanced.onlinelibrary.wiley.com/doi/10.1002/adsu.202500139 by Politecnico Di Torino Sist. Bibl Del Polit Di Torino, Wiley Online Library on [22/01/2026]. See the Terms and Conditions (https://onlinelibrary.wiley.com/terms-and-conditions) on Wiley Online Library for rules of use; OA articles are governed by the applicable Creative Commons License